HHS Public Access

Author manuscript

Langmuir. Author manuscript; available in PMC 2016 May 31.

Published in final edited form as:

Langmuir. 2012 December 11; 28(49): 17202–17210. doi:10.1021/la3031396.

Platinum Electrodeposition on Unsupported Carbon Nano-Onions

Diana Santiago[†], **Gabriel G. Rodríguez-Calero**[†], **Amit Palkar**[‡], **Diana Barraza-Jimenez**[§], **D. H. Galvan**[‖], **Gilberto Casillas**[⊥], **Alvaro Mayoral**[⊥,#], **Miguel Jose-Yacamán**[⊥], **Luis Echegoyen**[‡], and **Carlos R. Cabrera**[*,†]

[†]Center for Advanced Nanoscale Materials, Department of Chemistry, University of Puerto Rico, Rio-Piedras Campus, P.O. Box 23346, San Juan, Puerto Rico 00931

[‡]Department of Chemistry, University of Texas at El Paso, El Paso, Texas 79968-0519, United States

[§]Centro de Investigacioń en Alimentacioń y Desarrollo, A. C. Unidad Delicias, Av. 4[a] Sur 3820, Fracc. Vencedores del Desierto. Cd. Delicias Chih, México 33089

[‖]Centro de Nanociencias y Nanotecnología, Universidad Nacional Autonóma de Mésxico, Apartado Postal 2681, C. P. 22800, Ensenada, B. C., México 22800

[⊥]Physics and Astronomy Department, University of Texas at San Antonio, San Antonio, Texas 78249, United States

Abstract

An effort to develop smaller, well-dispersed catalytic materials electrochemically on high-surface-area carbon supports is required for improved fuel cell performance. A high-surface-area carbon material of interest is carbon nano-onions (CNOs), also known as multilayer fullerenes. The most convenient synthesis method for CNOs is annealing nanodiamond particles, thus retaining the size of the precursors and providing the possibility to prepare very small nanocatalysts using electrochemical techniques. In terms of pure metal catalysts, platinum is the most common catalyst used in fuel cells. The combination of Pt nanoparticles with CNOs could lead to new catalytic nanomaterials. In this work, this was accomplished by using a rotating disk–slurry electrode (RoDSE) technique. The Pt/CNO catalysts were prepared from slurries that contained functionalized CNOs and K_2PtCl_6 as the platinum precursor in aqueous 0.1 M H_2SO_4 solution. X-ray photoelectron spectroscopy results showed that 37% of the Pt on the CNOs is metallic Pt whereas 63% had higher binding energies, which is evidence of higher oxidation states or the presence of Pt atoms and clusters on CNOs. However, aberration-corrected scanning transmission electron microscopy of the Pt/CNOs confirmed the presence of Pt atoms and clusters on CNOs.

[*]**Corresponding Author:**; Email: carlos.cabrera2@upr.edu. Phone: (1) 787-764-0000 ext-4807. Fax: (1) 787-756-8242

[#]**Present Address**: Laboratorio de Microscopias Avanzadas, Instituto de Nanociencia de Aragon, Universidad de Zaragoza, 50018, Zaragoza, Spain.

Supporting Information

Additional computational studies for the first 10 orbitals of coronene and corannulene with Pt atoms and a relevant discussion. This material is available free of charge via the Internet at http://pubs.acs.org.

Notes

The authors declare no competing financial interest.

Thermal gravimetric analysis showed the excellent thermal stability of the Pt/CNOs and a lower onset potential for the electrochemical oxidation of methanol compared to that of commercial Pt/Vulcan catalyst material. The computational method confirmed the Pt atoms' location at CNOs surface sites. Geometric parameters for distances between Pt atoms in the 3Pt/CNOs molecular system from our theoretical calculations are in agreement with the respective parameters obtained experimentally. The combination of CNO with RoDSE presents a new highly dispersed catalyst nanomaterial.

Graphical abstract

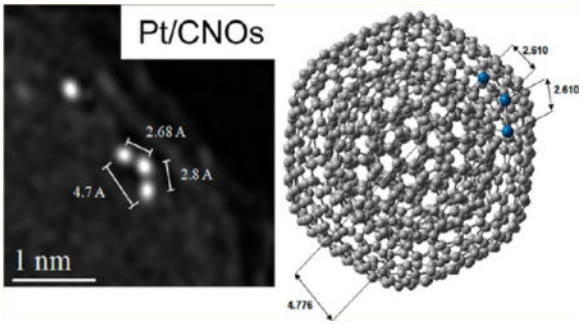

Since carbon nano-onions (CNOs) were discovered by Ugarte in 1992,[1] many researchers have tried to find different ways to synthesize them, to understand their growth mechanisms, and to increase their yields. CNOs, also known as onionlike or multilayer fullerenes (OLFs), are concentric fullerenes that ideally are composed of an inner shell of 60 carbon atoms (C_{60}) and the number of carbons in the other layers increases as $60n^2$, where n is the number of layers. The discovery of this new carbon material prompted the study of their properties and possible applications. For example, Joly-Pottuz et al. have studied the tribological properties of CNOs as potential lubricant additives.[2] CNOs also have been suggested for gas storage applications because of their very large surface areas[3] and proposed as materials for electromagnetic shielding because of the radicals trapped in their inner core by defect-free outer shells when the CNOs are synthesized by the annealing of nanodiamonds.[4]

The use of CNOs as a catalyst support for fuel cell applications was suggested in 2006[5] because CNOs have a higher surface area than single-walled carbon nanotubes (SWCNTs). The group of Guo and Xu et al. reported the preparation of Pt/OLF catalysts using the same impregnation-reduction method but using OLFs synthesized by different techniques. The OLFs prepared by arc discharge in water yielded Pt nanoparticles with an average diameter of 4.3 nm,[6] and the OLFs prepared by chemical vapor deposition formed nanoparticles of approximately 3 nm diameter.[7] These studies suggest a dependence of the platinum particle size deposited on the CNOs on the synthesis method used to grow the CNOs as well as on the Pt nanoparticle preparation method.

The size of the CNOs depends on the synthesis method and the carbon precursor. For example, CNOs between 5 and 50 nm were found when they were prepared via arc discharge of graphite under water using a current of 30 A,[8] which resulted in two types of CNOs: small ones (5 to 20 nm), which were well crystallized, and larger ones, which were

poorly crystallized. Recently, Chung et al. synthesized CNOs using flames modulated by acoustic excitation to produce CNOs of around 25 nm when low frequencies (f = 10 and 20 Hz) were used and sizes between 15 and 20 nm under higher frequencies (f = 60, 66, and 70).[9] The graphitization of the CNOs was higher for the CNOs prepared using low frequencies than when using higher frequencies. Another commonly used technique for preparing CNOs is chemical vapor deposition (CVD), a method that produces large amounts of very pure CNOs.[10] This method used alloys or compounds containing Fe as a catalyst among other elements,[10,11] and the final products were CNOs with catalyst cores. The diameters of these CNOs were in a broad range of 10–90 nm. Moreover, nanodiamond powder with diameters smaller than 10 nm has been used for CNO synthesis by annealing to produce CNO particles consisting of a few shells while maintaining the particle sizes of the precursor.[12] This synthesis method makes the CNO an attractive carbon support material to be studied.

Recently, Santiago et al. reported a new electrochemical method of Pt electrodeposition on high-surface-area carbon support materials such as Vulcan XC72.[13] The technique has been named the rotating disk–slurry electrode (RoDSE), which is a greener way to prepare bulk carbon-supported catalyst materials. The electrochemical deposition of Pt nanoparticles was reported for a slurry solution of Vulcan and K_2PtCl_6 in H_2SO_4, yielding polycrystalline Pt nanoparticles with an average size of 4 nm on Vulcan.[13] The present study describes the bulk preparation and characterization of Pt/CNOs prepared electrochemically using the RoDSE technique and its performance relative to that of Pt/Vulcan. Very small CNOs, such as those prepared by annealing nanodiamond particles, could aid in the electrochemical preparation of highly dispersed nanocatalysts for fuel cell applications. Palkar et al. have reported that small CNOs synthesized by this method are more reactive and thermodynamically stable than larger CNOs synthesized by the arcing graphite rod.[12] The combination of Pt deposition using RoDSE and CNOs prepared from nanodiamond resulted in a new thermally stable nanomaterial with highly disperse Pt atoms and clusters and, most importantly, with enhanced electrocatalytic activity for methanol oxidation.

EXPERIMENTAL SECTION

Methods

Preparation of the Pt/CNO Catalyst—CNOs with an average diameter of 5 nm were prepared by the thermal annealing of nanodiamond particles as previously described elsewhere.[12] The electrodeposition of Pt on CNOs was performed using the RoDSE technique developed and already reported by Santiago et al.[13] The same conditions used for the preparation of Pt/C using Vulcan XC-72R as the carbon support were used for the preparation of Pt/CNO. Briefly, a suspension was formed in a beaker with 50 mg of CNO and 20 mL of 0.10 M H_2SO_4 (Optima, Aldrich) and sonicated for 8 h. The resulting suspension was placed in the three-electrode cell for electroreductive deposition of platinum. The electrochemical cell had three compartments separated by fritted glass. A 5 mM K_2PtCl_6 (Aldrich) solution (2.00 mL) was then added to the suspension to form the slurry. Afterward, the electrochemical cell was sealed and purged with nitrogen for 1 h while the rotating disk electrode (RDE) (PINE Instruments) was rotated at 900 rpm in the slurry

solution. The disk electrode used, which also was used to apply the necessary potential, was a glassy carbon electrode with a geometric area of 0.20 cm^2. A graphite rod and a Ag/AgCl (+0.197 V vs NHE) electrode were used as the counter and reference electrodes, respectively. The electrodeposition to prepare the Pt/CNO was done by applying a constant potential of −0.200 V (Basic Electrochemical System of EG&G) for 2 h. The electrodeposition was stopped after the electrodeposition process was repeated three additional times. The platinum complex (2.00 mL of 5 mM K_2PtCl_6) was added to the slurry solution before each cycle was performed. Afterward, the final slurry was filtered and rinsed with 600 mL of nanopure water (18.2 MΩ cm NANOpure Diamond of Barnstead) and air dried before characterization.

Surface Analysis—The aberration-corrected scanning transmission electron microscope (STEM) analysis was done using a JEOL JEM-ARM200F at the University of Texas at San Antonio (UTSA). The microscope was operated at 200 kV, achieving a resolution of 0.08 nm. The convergence semiangle used was set to 24 mrad. STEM micrographs were acquired with an exposure pixel time of 20 μs in order to avoid damage to the sample. Annular dark field (ADF) images were collected with 20 and 27 inner and outer collection semiangles, and the bright field Rigaku Ultima III X-ray diffractometer system and Cu Kα radiation. Scans were recorded for a 2θ angle range between 20 and 140θ with a step size of 0.1° and a step time of 48 s. X-ray photoelectron spectroscopy (XPS) (PHI 5600ci) was performed with a Mg Kα monochromatic X-ray source (350 W) and a hemispherical electron energy analyzer. For XPS, a small amount of the catalytic powder was pressed onto a Mo film. The XPS results for the Pt 4f binding energy region were analyzed using a curve-fitting program (Multipack) for peak deconvolution. Thermogravimetric analysis (TGA) was done in air with a temperature ramp of 10 °C min^{-1}.

Electrochemical Measurements—All the electrochemical measurements were made using Ag/AgCl and a graphite rod as the reference and counter electrodes, respectively. A basic electrochemical system (EG&G) was used for all electrochemical experiments. All of the potentials measured in this study are referenced to Ag/AgCl. The working electrodes were prepared by placing a paste of the catalytic Pt/CNO on a glassy carbon electrode (3 mm diameter, Bioanalytical System), which was previously cleaned. The ink paste used for the electrode preparation consisted of a suspension with 1 mg of the Pt/CNOs nanocatalyst powder prepared by RoDSE, 8 μL of Nafion (Aldrich), and 250 μL of isopropanol that was ultrasonicated for 30 min. The electrodes were prepared by adding 8 μL of the ink paste to a glassy carbon electrode and drying in air for 15 min.

The cyclic voltammetric (CV) experiments of platinum supported on carbon were done in 0.5 M H_2SO_4 using a potential range of between −0.20 and 1.0 V and a sweep rate of 50 mV s^{-1}. The performance of the Pt/CNOs was compared against that of Pt/VXC (Pt/Vulcan, prepared similarly by the RoDSE technique) in sulfuric acid and for methanol oxidation studies using a nitrogen-saturated solution of 1 M CH_3OH/0.5 M H_2SO_4. Two electrochemical techniques were used: CV using a potential range between −0.20 and 1.0 V at a sweep rate of 50 mV s^{-1} and chronoamperometry by applying a constant potential of −0.50 V for 1 h.

Computational Analysis—Computational simulation calculations were made by employing the Gaussian 09[14] program suite. Three-layer CNOs arranged in the order C_{60}, C_{240}, and C_{540} were used. All calculations were carried out with ONIOM methodology.[15] Such methodology consists of taking the interaction components of interest in two or three different theoretical levels such as quantum mechanics and molecular mechanics QM/MM. The goal is to achieve good-precision calculations for the geometric parameters. However, the resulting energy values are only relative values. The theoretical level used in our calculations was functional density theory with the local density approximations that considers spin (LSDA).[16] The Dunning–Huzinaga D95[17] basis set was employed for carbon atoms, and the Stuttgart Dresden (SDD)[18] basis set was employed for Pt atoms. For the remaining C atoms of the CNOs, an MM-level application was used, including a universal force field (UFF).[19]

RESULTS AND DISCUSSION

The platinum nanoparticles electrodeposited on the CNOs, prepared by annealing nanodiamond particles, were expected to be smaller than the platinum nanoparticles electrodeposited on Vulcan (VXC). Compared to VXC, the CNOs prepared in this study are very small, almost 5 nm on average. The platinum electrodeposition on CNOs was expected to behave differently than that on VXC because of the difference in the carbon structure because VXC is an amorphous carbon form and CNOs have graphitic surfaces. However, the graphs for the electrodepositions (current vs time at a constant potential of −0.200 V) were similar for both carbon supports, showing that the RoDSE technique works equally well for different carbon supports (Figure 1).

X-ray photoelectron spectroscopy (XPS) analysis was done to determine the oxidation state of the platinum electrodeposited on the surface of the CNOs to determine how much of this platinum is in metallic form. Figure 2a shows the expected spectra of CNOs and Pt/CNOs, both having C (near to 284 eV) and O (near to 530 eV). A small peak in the binding energy region between 70 and 80 eV is also observed in the Pt/CNOs spectrum corresponding to the energy core level of Pt 4f. The high-resolution XPS of the Pt 4f region (Figure 2b) shows the expected doublet of platinum. Different oxidation states were found after the deconvolution of the doublet: Pt(0), Pt(II), and Pt(IV). The data obtained from the deconvolution are in Table 1, which shows the binding energies of each peak and their relative areas. The Pt $4f_{7/2}$ peak of lower binding energy is at 71.2 eV, which agrees with the values reported in the literature for Pt(0). The sums of the relative peak areas of $4f_{7/2}$ and $4f_{5/2}$ for Pt(0), Pt(II), and Pt(IV) are 37.1, 38.0, and 24.9%, respectively. These results show that 37.1% of the Pt on the CNOs is reduced to metallic Pt whereas 62.9% remains at a higher binding energy. One of the possible reasons for this observation is that the electrochemical deposition process combined with the hydrodynamic flow of the RoDSE technique does not allow for the complete reduction of platinum on the CNOs. However, as is shown in the HRTEM results, the higher binding energy may be due to the smaller Pt clusters and atoms on the CNOs. This higher binding energy effect has been observed with Pd clusters.[20]

The crystalline structure information and the average size of the platinum nanoparticles on the Pt/CNOs samples were obtained from XRD analysis. Figure 3 shows the XRD pattern of

the platinum nanoparticles, revealing six diffraction peaks of a face-centered-cubic crystalline structure corresponding to Miller indices (111), (200), (220), (311), (222), and (331). The platinum particle size was calculated to be 8 ± 2 nm using the Scherrer equation.[21] An additional XRD peak was found at 26° that corresponds to the crystalline structure of carbon with a Miller index of (002).

Thermogravimetric analysis (TGA) was done to observe the thermal stability of the samples in air and also to quantify the metal that is left when the carbon is completely oxidized. Figure 4 shows a comparison of the carbon supports, CNOs versus Vulcan (VCX), and the samples prepared using the RoDSE technique, Pt/CNOs versus Pt/VXC. Pure CNOs began to oxidize at 550 °C, which compares to 500 °C for VXC, but the CNOs were completely oxidized 50 °C lower than for VXC. Pt/VXC samples start decomposing near 400 °C whereas Pt/CNO samples decomposed 50 °C higher. Interestingly, both samples ended the carbon oxidation at the same temperature, while retaining the same weight percent, 11.5%. It is known that higher concentrations of metal on carbon supports accelerate carbon decomposition in air at lower temperatures whereas less metal on the carbon supports leads to oxidation at higher temperatures. Although both samples contained the same amount of electrodeposited platinum, Pt/CNOs were more thermally stable than Pt/VXC. This shows the importance of the carbon material structures in determining the thermal stabilities.

Two different domains are observed for the carbon decomposition of Pt/VXC samples. First, a sharp decrease in weight occurs at around 450 °C, and a second, slower mass decrease occurs between 450 and 625 °C. These observations were discussed in our previous article as resulting from the preparation method using the RoDSE technique. Interestingly, the oxidation of Pt/CNO samples does not exhibit the slow mass decrease in the usual carbon oxidation temperature region. Previous to the electrodeposition of platinum, pretreatment of the carbon materials in low-concentration acid was done to disperse them in the slurries by surface oxidation. This pretreatment could be the reason that the Pt/VXC samples show this behavior whereas Pt/CNOs exhibit better stability after oxidation, exhibiting similar behavior to that of plain CNOs.

High-resolution TEM analysis was necessary for these samples because of the very small sizes of the particles. Figure 5a is a bright-field (BF) micrograph where a clear structure of one CNO with 12 layers can be seen. In an annular dark field (ADF) micrograph (Figure 5b), some very bright and disorganized spots can be distinguished. The intensity in the ADF images is proportional to the Z number of the atoms, indicating that the bright spots correspond to heavy atoms, corresponding to Pt in this case. These atoms could be ionic or electrodeposited Pt atoms on the CNOs. In other micrographs, Pt nanoparticles were observed. Figure 5c,d corresponds to ADF and BF micrographs in the same area. In the micrographs shown in Figure 5c,d, the Pt nanoparticles are the bright areas (Figure 5c) and differences in the lattice parameters between the Pt and carbon regions are observed (Figure 5d).

Electrochemical characterization was done to compare Pt/CNOs versus Pt/VXC that were prepared by the same RoDSE method. Figure 6a shows defined peaks for the hydrogen adsorption and desorption area on the platinum surface for Pt/CNOs and Pt/VXC and no

peaks for the CNO electrode. The active surface areas of Pt were estimated by integrating the hydrogen adsorption area in sulfuric acid (Figure 6a) to normalize the currents in the cyclic voltammograms. The Pt/VXC and Pt/CNO samples had similar hydrogen adsorption/desorption peaks in sulfuric acid. For the methanol oxidation voltammograms (Figure 6b), Pt/CNOs had a lower onset potential, at 0.2 V, than Pt/VXC. One of the reasons for this behavior may be due to the Pt atom and clusters seen in the Pt/CNO samples as well as to the higher thermal stability. However, a more negative onset potential of the Pt/CNOs sample may be associated with the use of CNOs as a carbon support.

COMPUTATIONAL STUDY OF CNOS AND PT/CNOS

A computational analysis was done using two structural models for the CNO outer layer, with the goal of comparing the geometric parameters as well as the resulting energy values. The first model selected contained a coronene unit as the supporting base for the Pt atoms. Geometric optimization was initially obtained followed by vibrational frequency calculations to confirm that the structures do not have imaginary frequencies (which are associated with transition states). The same calculation was performed for each one of the CNO structures with one, two, and three Pt atoms, which we have labeled 1Pt/CNO, 2Pt/CNO, and 3Pt/CNO, respectively.

The second structural motif used for the calculation was corannulene instead of coronene as the supporting structures for Pt atoms on the exterior layer of CNOs. Figures 7 and 8 show the bond lengths for the optimized systems at the QM level. Figure 9 is a scheme of the complete structure containing both atoms at the QM and MM levels.

Both structures, coronene and corannulene, have a shorter C–Pt bond length when using two Pt atoms. However, for all calculations using one to three Pt atoms, shorter C–Pt bond lengths were always observed for the corannulene. Likewise, we observed that both Pt–Pt and C–Pt bond lengths were symmetrical for the coronene and the corannulene. Pt–Pt bond lengths are slightly longer for the corannulene system. Meanwhile, the opposite happened for the C–Pt bond lengths because they are slightly longer for the CNOs with coronene.

Table 2 shows the bond lengths for optimized structures using a central hexagon as well as a pentagon with values for the isolated system and for the system containing one to three Pt atoms. The calculation for the differences in bond length in CNO structures and structures containing Pt atoms showed that the structure with corannulene had, for all bond lengths, a larger difference when compared to structures without Pt. Table 3 summarizes the energy data for the frontier orbitals, the HOMO–LUMO energy, as well as the stability values for the coronene and corannulene systems. Stability calculations were carried out using eq 1

$$S=\frac{[E_{(\mathrm{CNO+Pt})}-E_{(\mathrm{CNO})}-E_{(\mathrm{Pt\ atoms})}]}{\text{number of Platinum atoms}} \quad (1)$$

where S represents the system stability for CNO structures containing Pt, where E is for each energy term, including CNO systems containing Pt, isolated CNOs, and Pt atoms.

The stability values associated with the distance modifications on the central hexagon and pentagon bond lengths in the selected systems are shown in Figures 7 and 8. These stability values are more negative for the system containing the corannulene if compared to the structure containing the coronene. A negative value in the stability represents how Pt atoms gradually stabilize the system as the number of Pt atoms increases.

The HOMO value for CNOs, possessing a corannulene unit had a lower energy when compared to CNOs containing a coronene, before including the Pt atoms. This higher energy, for the system with the coronene, is associated with a higher electron-donation capability. When the first Pt atom is added, the HOMO energy increases to 1.137 eV for the corannulene. However, for the CNO containing the coronene, the HOMO increases only by 0.519 eV. For both CNO systems, the increasing trend in HOMO energy diminishes as the number of Pt atoms increases. The LUMO energies exhibited a larger decrease when the first Pt atom was added to the structure containing the coronene rather than the structure containing the corannulene. The difference was smaller when comparing both structures to one to three Pt atoms. The corannulene and coronene units had a similar decreasing LUMO trend. HOMO–LUMO energies decreased for both systems, with a single Pt atom, to 1.622 and 2.050 eV for coronene and corannulene, respectively.

Analyzing the HOMO–LUMO values, we found that both coronene and corannulene had decreased values, indicating that CNOs behave as semiconductors. As Pt atoms are added to the CNOs, the HOMO–LUMO gap decreases until it reaches semimetallic (0.113 and 0.084 eV) energy gaps.

It is possible to find catalytic systems[22] that initially show semiconductor behavior and can be modified to exhibit metallic behavior. This change could be correlated to the enhanced catalytic activity and thermal stability, as was reported by Galvan et al. for MoS_2 clusters[23] and in this work for methanol oxidation.

CONCLUSIONS

The unsupported electrodeposition of Pt on CNOs, using the rotating disk–slurry electrode (RoDSE) technique, may be considered to be a promising approach to the mass production of platinum atoms and cluster-carbon-supported catalysts for fuel cell applications. CNOs were synthesized by annealing nanodiamond powder and subjected to acid treatment to increase their surface oxygen functionalities in order to facilitate platinum electrodeposition. The electrodeposition process behaves similarly to that for Vulcan as a carbon support. The quantity of Pt electrodeposited (i.e., metal loading) on Pt/CNOs is similar to that for samples prepared using Vulcan (i.e., 11.5 wt %) as identified by TGA analysis. Although both Pt/CNOs and Pt/VXC have the same metal loading, the CNO samples exhibited enhanced thermal stability. The HRTEM images showed the presence of dispersed Pt clusters and atoms on the CNOs. The electrochemical analysis showed active platinum electrodeposited on CNOs with defined hydrogen adsorption–desorption peaks, showing enhanced onset potentials for methanol electrooxidation. Theoretical calculations showed the possibility of incorporating Pt atoms into carbon nano-onion systems. Theoretical results for CNOs, with three Pt atoms, are in agreement with experimental HRTEM results. According to 3Pt/CNO

geometric parameters obtained from the experimental study, we believe that Pt atoms are bonded to a hexagonal ring, and this is in agreement with stability data obtained in this work. CNO systems with a coronene group favor system stability. Lower LUMO energy values were observed for the corannulene system, which favor the attachment of the first Pt atom, the 1Pt/CNO system. Not surprisingly, as additional Pt atoms are added to the CNOs, the system becomes more metallic. Calculated bond distances between Pt–Pt were very similar to those seen in the HRTEM images. These structural motifs may explain the improved thermal stability and lower methanol oxidation onset potentials. Optimizing the RoDSE technique using CNOs may pave the way to preparing bulk quantities of highly active supported metal atom and cluster catalysts for fuel cell applications.

Supplementary Material

Refer to Web version on PubMed Central for supplementary material.

Acknowledgments

This work was financially supported by the NASA-URC Center for Advanced Nanoscale Materials under grant no. NNX10AQ17A. The authors would like to acknowledge The Welch Foundation Agency, project AX-1615: Controlling the Shape and Particles Using Wet Chemistry Methods and Its Application to Synthesis of Hollow Bimetallic Nanostructures; the National Science Foundation (NSF) PREM grant number DMR-0934218: Oxide and Metal Nanoparticles: The Interface between life sciences and physical sciences; and CONACYT-Mexico grant number 106437. The authors would also like to thank the International Center for Nanotechnology and Advanced Materials (ICNAM) at UTSA, the RCMI Center for Interdisciplinary Health Research (CIHR), and the project award number 2G12RR013646-11 from the National Center for Research Resources. L.E. thanks the Robert A. Welch Foundation for an endowed chair (grant no. AH-0033) and the U.S. NSF (grant no. CHE-1110967) for the generous support of his work. D.H.G. acknowledges El Departamento de Supercomputo-UNAM for the facilities provided to perform the calculations. D.B.-J. thanks CIMAV and Dr. Daniel Glossman-Mitnik for the facilities provided to visualize the structures. D.S. acknowledges the financial support of the Puerto Rico Space Grant Consortium and the AGEP-NSF Fellowship program. We also thank Dr. Michael Pelsozy for the TGA data, Dr. Esteban Faccini for the XPS data, and Harry Rivera for the XRD data.

References

1. Ugarte D. Curling and Closure of Graphitic Networks Under Electron-Beam Irradiation. Nature. 1992; 359:707–709. [PubMed: 11536508]
2. (a) Joly-Pottuz L, Vacher B, Ohmae N, Martin JM, Epicier T. Anti-Wear and Friction Reducing Mechanisms of Carbon Nano-Onions as Lubricant Additives. Tribol ett. 2008; 30:69–80.(b) Joly-Pottuz L, Vacher B, Le Mogne T, Martin JM, Mieno T, He CN, Zhao NQ. The Role of Nickel in Ni-Containing Nanotubes and Onions as Lubricant Additives. Tribol ett. 2008; 29:213–219.(c) Joly-Pottuz L, Bucholz EW, Matsumoto N, Phillpot SR, Sinnott SB, Ohmae N, Martin JM. Friction Properties of Carbon Nano-Onions from Experiment and Computer Simulations. Tribol ett. 2010; 37:75–81.
3. Sano N, Wang H, Alexandrou I, Chhowalla M, Teo KBK, Amaratunga GAJ, Iimura K. Properties of Carbon Onions Produced by an Arc Discharge in Water. J Appl Phys. 2002; 92:2783–2788.
4. Langlet R, Lambin P, Mayer A, Kuzhir PP, Maksimenko SA. Dipole Polarizability of Onion-Like Carbons and Electromagnetic Properties of Their Composites. Nanotechnology. 2008; 19:11.
5. Rettenbacher AS, Elliott B, Hudson JS, Amirkhanian A, Echegoyen L. Preparation and Functionalization of Multilayer Fullerenes (Carbon Nano-Onions). Chem—Eur J. 2006; 12:376–387. [PubMed: 16189840]
6. Guo JJ, Yang XW, Yao YL, Wang XM, Liu XG, Xu BS. Pt/Onion-Like Fullerenes as Catalyst for Direct Methanol Fuel Cell. Rare Met. 2006; 25:305–308.
7. Xu BS, Yang XW, Wang XM, Guo JJ, Liu XG. A Novel Catalyst Support for DMFC: Onion-Like Fullerenes. J Power Sources. 2006; 162:160–164.

8. Roy D, Chhowalla M, Wang H, Sano N, Alexandrou I, Clyne TW, Amaratunga GAJ. Characterisation of Carbon Nano-Onions Using Raman Spectroscopy. Chem Phys ett. 2003; 373:52–56.

9. Chung DH, Lin TH, Hou SS. Flame Synthesis of Carbon Nano-Onions Enhanced by Acoustic Modulation. Nanotechnology. 2010; 21:43.

10. Kang JL, Li JJ, Du XW, Shi CS, Zhao NQ, Nash P. Synthesis of Carbon Nanotubes and Carbon Onions by CVD Using a Ni/Y Catalyst Supported on Copper. Mater Sci Eng, A. 2008; 475:136–140.

11. (a) Zhang CG, Li JJ, Shi CS, Liu EZ, Du XW, Feng W, Zhao NQ. The Efficient Synthesis of Carbon Nano-Onions Using Chemical Vapor Deposition on an Unsupported Ni-Fe Alloy Catalyst. Carbon. 2011; 49:1151–1158.(b) Yang YZ, Liu XG, Guo XM, Wen HR, Xu BS. Synthesis of Nano Onion-Like Fullerenes by Chemical Vapor Deposition Using an Iron Catalyst Supported on Sodium Chloride. J Nanopart Res. 2011; 13:1979–1986.

12. Palkar A, Melin F, Cardona CM, Elliott B, Naskar AK, Edie DD, Kumbhar A, Echegoyen L. Reactivity Differences Between Carbon Nano Onions (CNOs) Prepared by Different Methods. Chem –Asian J. 2007; 2:625–633. [PubMed: 17465408]

13. Santiago D, Rodríguez-Calero GG, Rivera H, Tryk DA, Scibioh MA, Cabrera CR. Platinum Electrodeposition at High Surface Area Carbon Vulcan-XC-72R Material Using a Rotating Disk-Slurry Electrode Technique. J Electrochem Soc. 2010; 157:F189–F195.

14. Frisch, MJ.; Trucks, GW.; Schlegel, HB.; Scuseria, GE.; Robb, MA.; Cheeseman, JR.; Scalmani, G.; Barone, V.; Mennucci, B.; Petersson, GA.; Nakatsuji, H.; Caricato, M.; Li, X.; Hratchian, HP.; Izmaylov, AF.; Bloino, J.; Zheng, G.; Sonnenberg, JL.; Hada, M.; Ehara, M.; Toyota, K.; Fukuda, R.; Hasegawa, J.; Ishida, M.; Nakajima, T.; Honda, Y.; Kitao, O.; Nakai, H.; Vreven, T.; Montgomery, JJA.; Peralta, JE.; Ogliaro, F.; Bearpark, M.; Heyd, JJ.; Brothers, E.; Kudin, KN.; Staroverov, VN.; Kobayashi, R.; Normand, J.; Raghavachari, K.; Rendell, A.; Burant, JC.; Iyengar, SS.; Tomasi, J.; Cossi, M.; Rega, N.; Millam, NJ.; Klene, M.; Knox, JE.; Cross, JB.; Bakken, V.; Adamo, C.; Jaramillo, J.; Gomperts, R.; Stratmann, RE.; Yazyev, O.; Austin, AJ.; Cammi, R.; Pomelli, C.; Ochterski, JW.; Martin, RL.; Morokuma, K.; Zakrzewski, VG.; Voth, GA.; Salvador, P.; Dannenberg, JJ.; Dapprich, S.; Daniels, AD.; Farkas, Ö.; Foresman, JB.; Ortiz, JV.; Cioslowski, J.; Fox, DJ. Gaussian 09. Gaussian, Inc; Wallingford, CT: 2009. Revision A.1

15. (a) Svensson M, Humbel S, Froese RDJ, Matsubara T, Sieber S, Morokuma K. ONIOM: A Multilayered Integrated MO+MM Method for Geometry Optimizations and Single Point Energy Predictions. A Test for Diels-Alder Reactions and Pt(P(t-Bu)(3)) (2)+H-2 Oxidative Addition. J Phys Chem. 1996; 100:19357–19363.(b) Dapprich S, Komaromi I, Byun KS, Morokuma K, Frisch MJ. A New ONIOM Implementation in Gaussian98. Part I. The Calculation of Energies, Gradients, Vibrational Frequencies and Electric Field Derivatives. J Mol Struct: THEOCHEM. 1999; 461:1–21.

16. (a) Vosko SH, Wilk L, Nusair M. Accurate Spin-Dependent Electron Liquid Correlation Energies for Local Spin-Density Calculations – A Critical Analysis. Can J Phys. 1980; 58:1200–1211.(b) Painter GS. Density Functional Description of Molecular Bonding within the Local Spin-Density Approximation. J Phys Chem. 1986; 90:5530–5535.

17. Dunning, TH.; Hay, PJ. Modern Theoretical Chemistry. Vol. 3. Plenum; New York: 1976.

18. Nicklass A, Dolg M, Stoll H, Preuss H. AB-Initio Energy-Adjusted Pseudopotentials for the Noble-Gases Ne Through Xe -Calculation of Atomic Dipole and Quadrupole Polarizabilities. J Chem Phys. 1995; 102:8942–8952.

19. (a) Rappe AK, Casewit CJ, Colwell KS, Goddard WA, Skiff WM. UFF, a Full Periodic-Table Force-Field for Molecular Mechanics and Molecular-Dynamics Simulations. J Am Chem Soc. 1992; 114:10024–10035.(b) Rappe AK, Colwell KS, Casewit CJ. Application of a Universal Force-Field to Metal-Complex. Inorg Chem. 1993; 32:3438–3450.

20. (a) Diaz-Ayala R, Arroyo L, Raptis R, Cabrera CR. Thermal Reduction of Pd Molecular Cluster Precursors at Highly Ordered Pyrolytic Graphite Surfaces. Langmuir. 2004; 20:8329–8335. [PubMed: 15350110] (b) Kaden WE, Wu TP, Kunkel WA, Anderson SL. Electronic Structure Controls Reactivity of Size-Selected Pd Clusters Adsorbed on TiO(2) Surfaces. Science. 2009; 326:826–829. [PubMed: 19892976]

21. Bayati M, Abad JM, Bridges CA, Rosseinsky MJ, Schiffrin DJ. Size Control and Electrocatalytic Properties of Chemically Synthesized Platinum Nanoparticles Grown on Functionalised HOPG. J Electroanal Chem. 2008; 623:19–28.

22. (a) Bollinger MV, Lauritsen JV, Jacobsen KW, Norskov JK, Helveg S, Besenbacher F. One-Dimensional Metallic Edge States in MoS_2. Phys Rev ett. 2001; 87:19.(b) Byskov LS, Norskov JK, Clausen BS, Topsoe H. Edge Termination of MoS_2 and CoMoS Catalyst Particles. Catal ett. 2000; 64:95–99.(c) Helveg S, Lauritsen JV, Laegsgaard E, Stensgaard I, Norskov JK, Clausen BS, Topsoe H, Besenbacher F. Atomic-Scale Structure of Single-Layer MoS_2 Nanoclusters. Phys Rev ett. 2000; 84:951–954.(d) Carlsson A, Brorson M, Topsoe H. Morphology of WS(2) Nanoclusters in WS(2)/C Hydrodesulfurization Catalysts Revealed by High-Angle Annular Dark-Field Scanning Transmission Electron Microscopy (HAADF-STEM) Imaging. J Catal. 2004; 227:530–536.

23. Galvan DH, Amarillas AP, Jose-Yacaman M. Metallic States at the Edges of MoS(2) Clusters. Catal ett. 2009; 132:323–328.

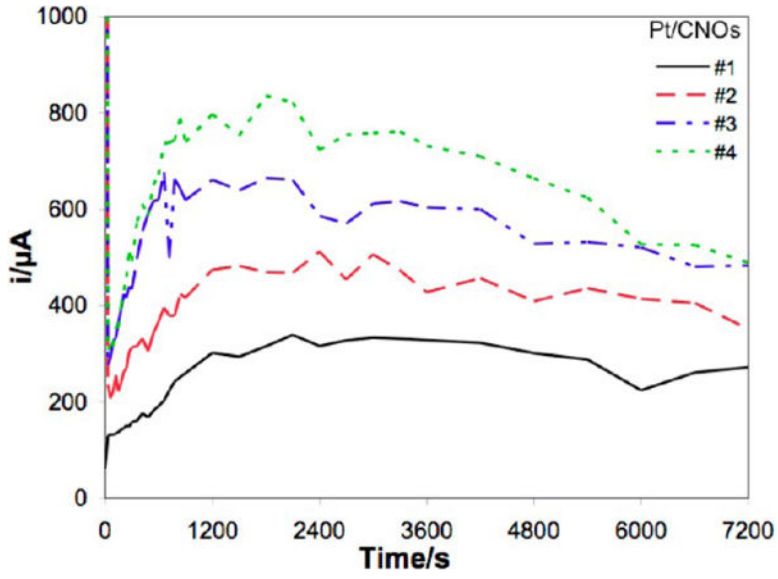

Figure 1.

Four-step electrodeposition of platinum on CNOs using the RoDSE technique: step 1 (black solid line), step 2 (red long-dashed line), step 3, (blue long- and short-dashed line), and step 4 (green short-dashed line).

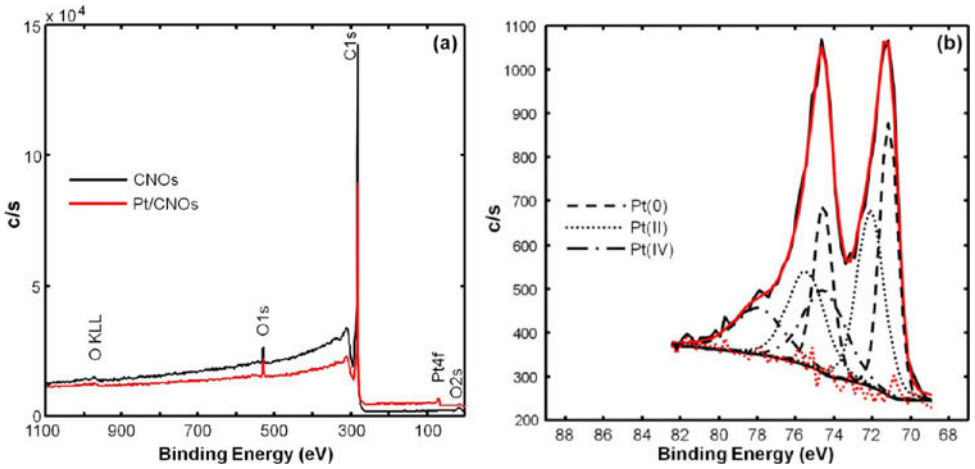

Figure 2.

X-ray photoelectron spectroscopy (XPS) spectrum of (a) CNOs and Pt/CNOs and (b) XPS high-resolution spectra of the Pt 4f binding-energy region of the Pt/CNOs sample.

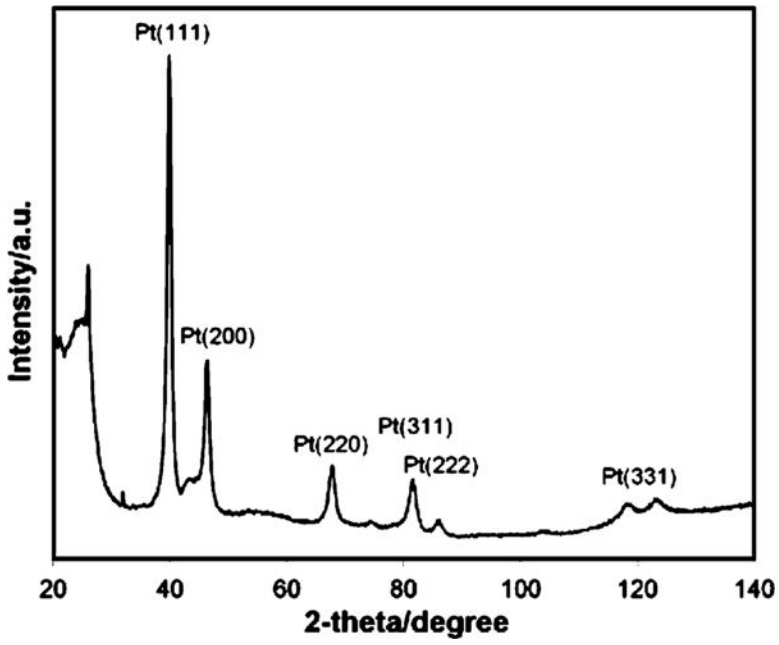

Figure 3.
X-ray diffraction (XRD) pattern of Pt/CNOs.

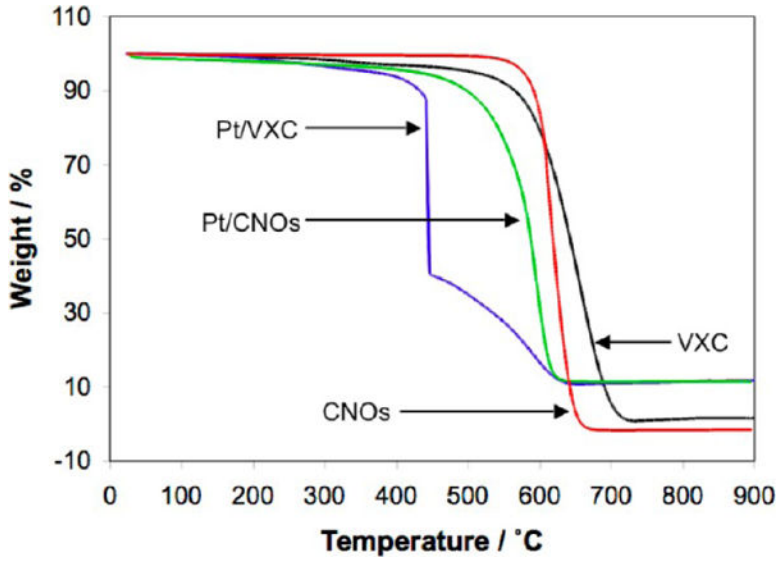

Figure 4.

Thermogravimetric analysis of Vulcan (VXC, black line), CNOs (red line), Pt/VXC (blue line), and Pt/CNOs (green line).

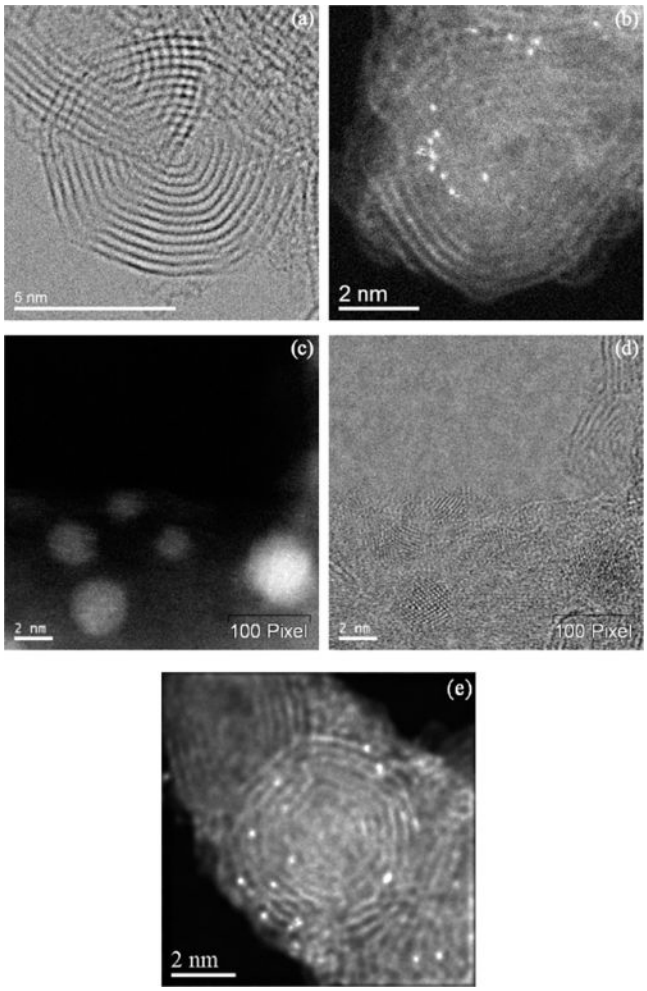

Figure 5.
High-resolution STEM images of the Pt/CNOs sample: (a, d) bright-field micrographs and (b, c, and e) dark-field micrographs.

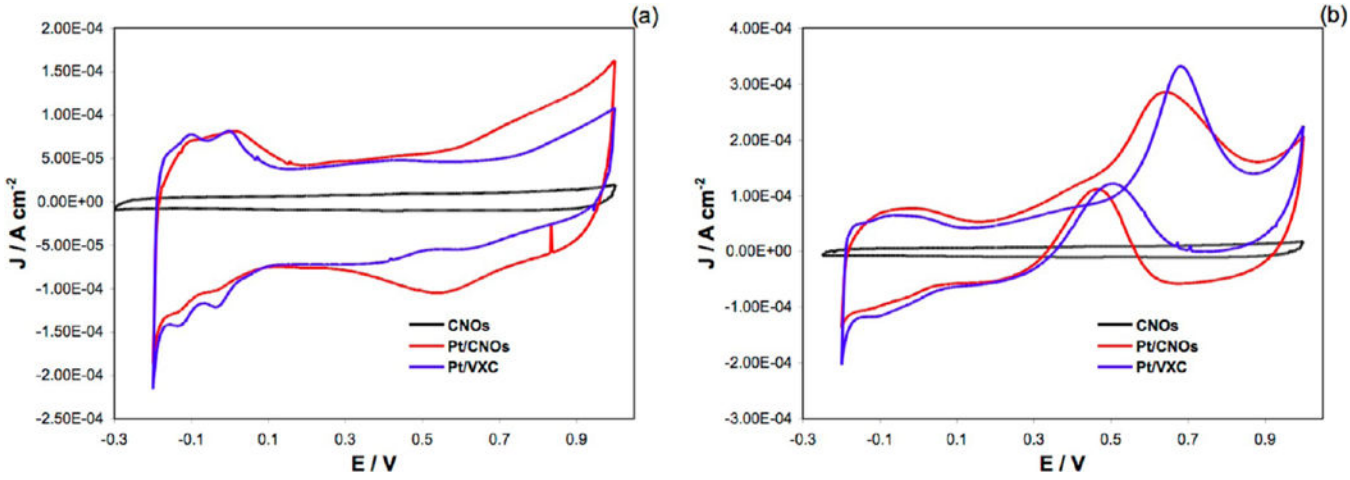

Figure 6.

Cyclic voltammetry of CNOs, Pt/CNOs, and Pt/VXC on (a) 0.5 M H_2SO_4 and (b) 1.0 M CH_3OH/0.5 M H_2SO_4 using a sweep rate of 50 mV s^{-1}.

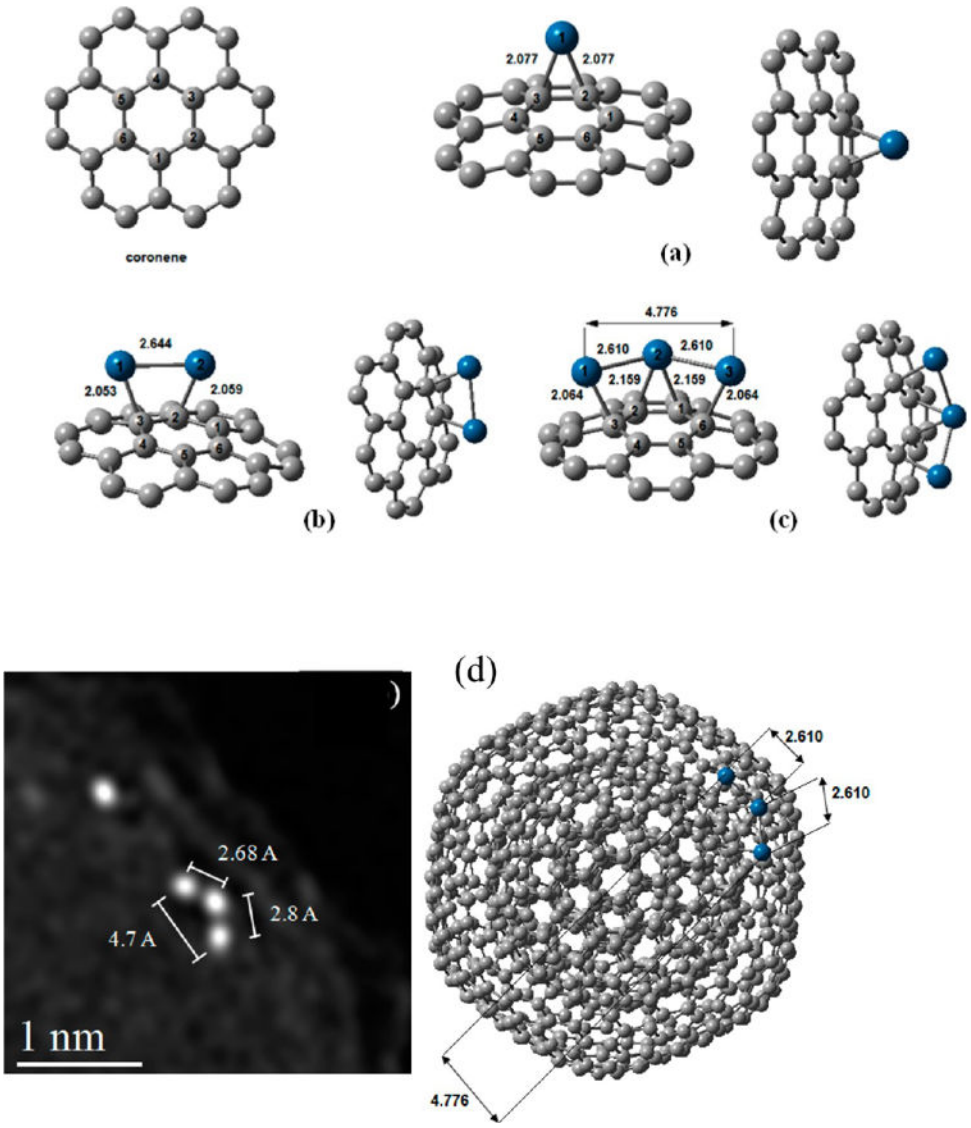

Figure 7.

System with a coronene unit with atom numbering at the central hexagon. Structures with optimized geometries for a coronene unit with C–Pt and Pt–Pt bond lengths: (a) 1Pt/CNOs, (b) 2Pt/CNOs, and (c) 3Pt/CNOs. (d, left) ADF STEM image of a cluster of three Pt atoms with distances in angstroms. The STEM data was filtered using the Richardson–Lucy algorithm implemented by Ichizuka to increase the accuracy in the measurement of the position of the atoms. DeConvHAADF is commercially available from HREM Research Inc. (www.hremresearch.com).

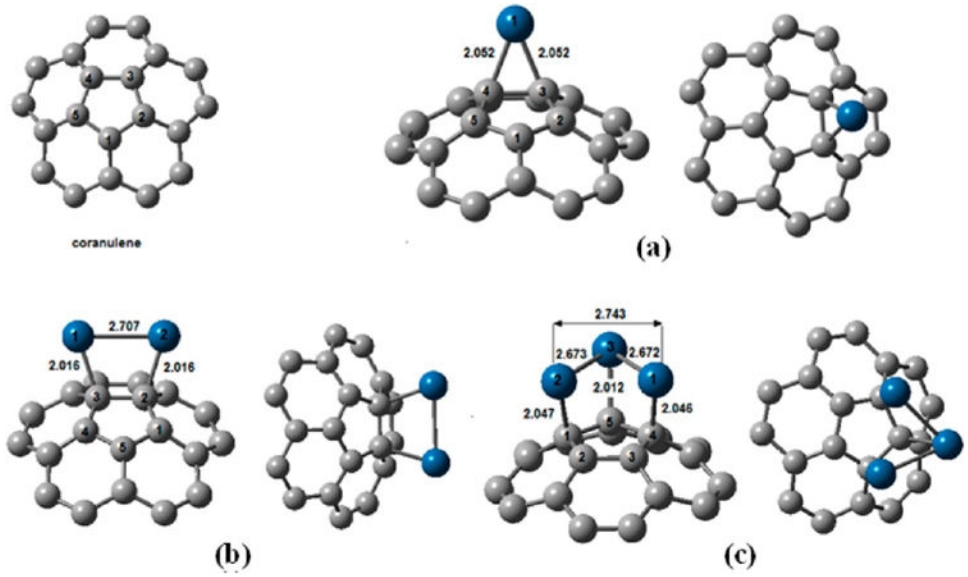

Figure 8.

System with corannulene support with atom numbering at the central hexagon. Structures with geometry optimization for corannulene support systems with C–Pt and Pt–Pt bond lengths: (a) CNOs 1Pt, (b) CNOs 2Pt, and (c) CNO 3Pt. Distances are in angstroms.

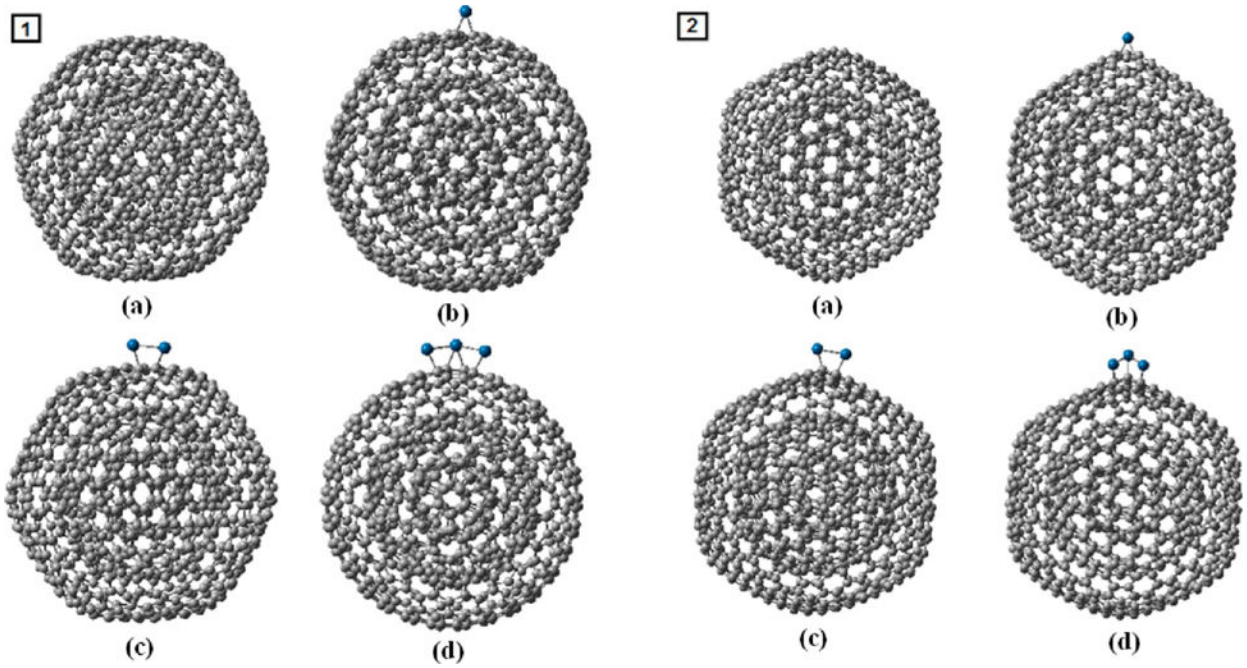

Figure 9.

CNOs after geometry optimization. (1) With the coronene unit: (a) CNO without Pt, (b) 1Pt/CNO, (c) 2Pt/CNO, and (d) 3Pt/CNO. (2) Corannulene unit: (a) CNO without Pt, (b) 1Pt/CNO, (c) 2Pt/CNO, and (d) 3Pt/CNO.

Table 1

X-ray Photoelectron Spectroscopy Binding Energies and Relative Peak Areas Obtained from the Deconvolution of the High-Resolution Pt 4f Spectra of Pt/CNOs

	binding energy		
sample	**$4f_{7/2}$**	**$4f_{5/2}$**	**relative peak area (%)**
Pt/CNOs	71.2	74.5	37.1
	72.1	75.4	38.0
	74.6	77.9	77.9

Table 2

Bond Lengths (Å) and Absolute Differences (Å) between CNOs (without Pt) and CNOs with $Pt_{1–3}$ Atoms Located at a Coronene[(a)] Central Hexagon or a Corannulene[(b)] Central Pentagon[a]

bond	bond length CNOs	CNOs-1Pt/CNOs	bond length 1Pt/CNOs	CNOs-2Pt/CNOs	bond length 2Pt/CNOs	CNOs-3Pt/CNOs	bond length 3Pt/CNOs
C(1)–C(2)[(a)]	1.433	0.027	1.460	0.055	1.488	0.053	1.486
C(2)–C(3)[(a)]	1.427	0.056	1.483	0.055	1.482	0.050	1.477
C(3)–C(4)[(a)]	1.432	0.028	1.460	0.030	1.462	0.033	1.465
C(4)–C(5)[(a)]	1.427	0.007	1.420	0.008	1.419	0.016	1.411
C(5)–C(6)[(a)]	1.432	0.009	1.441	0.005	1.437	0.034	1.466
C(6)–C(1)[(a)]	1.426	0.006	1.420	0.011	1.437	0.051	1.477
C(1)–C(2)[(b)]	1.419	0.005	1.414	0.023	1.442	0.043	1.462
C(2)–C(3)[(b)]	1.421	0.026	1.447	0.068	1.489	0.024	1.445
C(3)–C(4)[(b)]	1.421	0.079	1.500	0.021	1.442	0.041	1.462

[a]LSDA/D95 for carbon atoms and LSDA/SDD for Pt atoms.

Table 3

Energy of the HOMO, LUMO, HOMO–LUMO, and Stabilitiy Values (eV) for the Two Systems of Interest: (a) Coronene and (b) Corannulene[a]

	HOMO		LUMO		HOMO–LUMO		S	
structure	**(a)**	**(b)**	**(a)**	**(b)**	**(a)**	**(b)**	**(a)**	**(b)**
CNOs	−5.752	−6.248	−2.906	−3.039	2.846	3.209		
1Pt/CNOs	−5.233	−5.111	−4.010	−3.952	1.223	1.159	−8.633	−9.509
2Pt/CNOs	−4.755	−4.545	−4.258	−4.099	0.498	0.446	−6.276	−6.983

[a]Calculations are made using LSDA/D95 for carbon atoms and LSDA/SDD for Pt atoms.